Title

Global morphodynamic response of deltas to sea-level rise in the 21st century

Authors

Jaap H. Nienhuis[1,*], Roderik S.W. van de Wal[1,2]

Affiliations

[1]Department of Physical Geography, Utrecht University, Utrecht, NL

[2]Institute for Marine and Atmospheric Research, Utrecht University, Utrecht, NL

*corresponding author address: Princetonlaan 8a, 3584 CB, Utrecht, j.h.nienhuis@uu.nl

Abstract

River deltas will likely experience significant land loss because of relative sea-level rise (RSLR), but predictions have remained elusive. Here, we use global data of RSLR and river sediment supply to build a validated model of delta response to RSLR for all ~10,000 deltas globally. Applying this model to predict future delta change, we find that all IPCC RCP sea-level scenarios lead to a net delta loss by the end of the 21st century, ranging from -52 ± 36 (1 s.d.) km^2yr^{-1} for RCP2.6 to -808 ± 80 km^2yr^{-1} for RCP8.5. We find that river dams, subsidence, and sea-level rise have had a comparable influence on reduced delta growth over the past decades, but that by 2100 under RCP8.5 more than 80% of delta land loss will be caused by climate-change driven sea-level rise.

Main text

River deltas are low-lying coastal landforms created by fluvial sediment deposition. Delta shorelines can retreat landward through relative sea-level rise (RSLR) but also advance seaward through sedimentation and delta plain aggradation. These dynamics are widely acknowledged and observed in field and experimental studies (1–5). Currently, however, most future projections of delta land loss from RSLR ignore the potential for erosion and sedimentation (6), following a so-called "bath-tub" or passive flood mapping approach (e.g., 7, 8) that remains unvalidated by observations. The potential for delta sedimentation is apparent because, despite sea-level rise, deltas globally have gained land in recent decades (9).

Over the past decades, morphodynamic models (4, 10, 11), physical experiments (12, 13) and field studies (14) have shown how fluvial sediment supply and sea-level change control delta morphology (Fig. 1a, 1b). Fluvial sediment delivered to a delta is partitioned between delta plain aggradation, shoreline progradation, and loss to the offshore (5, 12, 15). Morphodynamic feedbacks arise from the response of sediment partitioning to delta morphology (16). Under rising sea-level, fluvial sediments will aggrade the delta plain up to a certain distance upstream (5). Fast RSLR can force a scenario of rapid shoreline erosion if all sediment is deposited on the delta plain and no sediment is left to supply the delta shoreline. Similarly, reductions in fluvial sediment supply to river deltas (e.g. resulting from dams, sand mining (17)) can decrease natural delta land gain rates (9, 18).

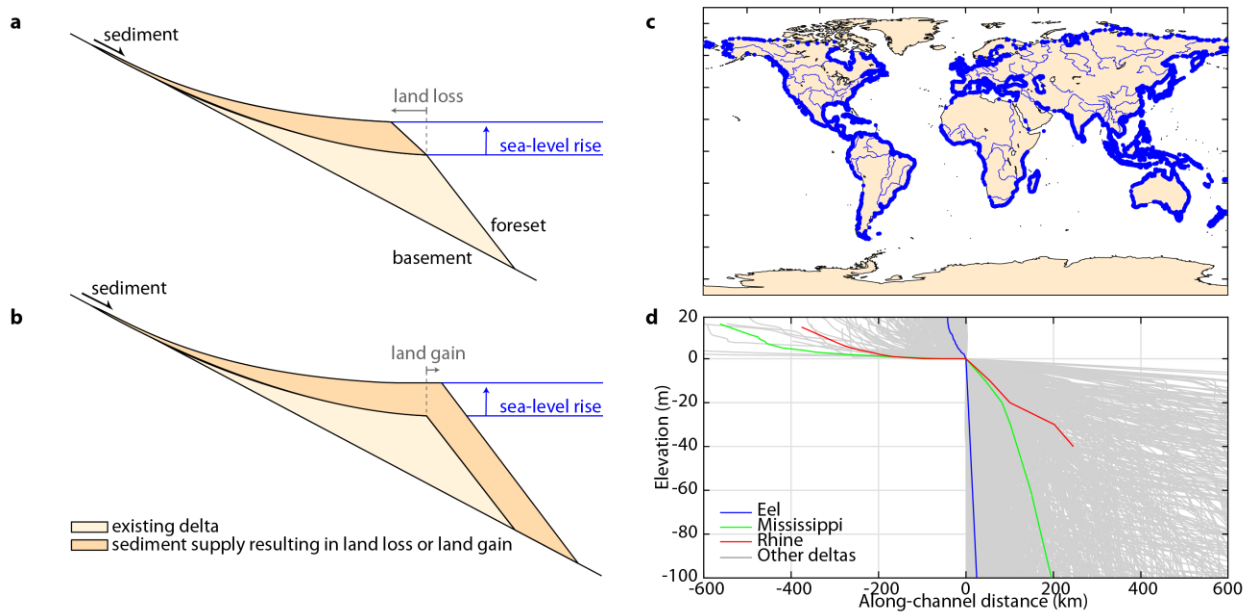

Figure 1: Delta profile response to relative sea-level rise. Model schematization for relatively (**a**) low, and (**b**) high fluvial sediment supply, resulting in land loss and land gain, respectively. (**c**) locations, and (**d**) longitudinal profiles of all (n = 10,848) coastal deltas globally, from (9).

Here, we apply a morphodynamic model to investigate land area change of 10,848 deltas (Fig. 1c) for various representative concentration pathway (RCP) scenarios of sea-level rise (Fig. 1c, 1d). Our model compares width-averaged bed- and suspended load sediment supply against local subsidence and sea-level rise, which together constitute RSLR. Based on the present-day delta longitudinal profile (Fig. 1d), we can then predict shoreline retreat (Fig. 1a) or advance (Fig. 1b).

Our global scale allows us to investigate drivers and trends that would be obscured in studies considering a single delta. For example, it is unknown to what extent subsidence drives the ongoing Mississippi River delta land loss. Using our morphodynamic model we can separate individual drivers and help improve predictions in case such drivers change into the future.

We validate our model against observed delta change from 1985-2015 (19) using estimates of subsidence (20), sea-level change (21), and fluvial sediment supply (22) for 10,848 deltas. We find that shoreline change predictions are generally the correct order of magnitude, and that our model explains a substantial fraction (R^2 = 0.4, Skill Score = 0.2) of delta land loss and land gain. The explained variance increases rapidly if the only larger deltas are selected, suggesting that a part of the past trend is still too small to be explained by the four processes captured in the current analysis (Fig. S4). We assess model and data uncertainty by means of a Monte Carlo method as described in the Supplementary Materials.

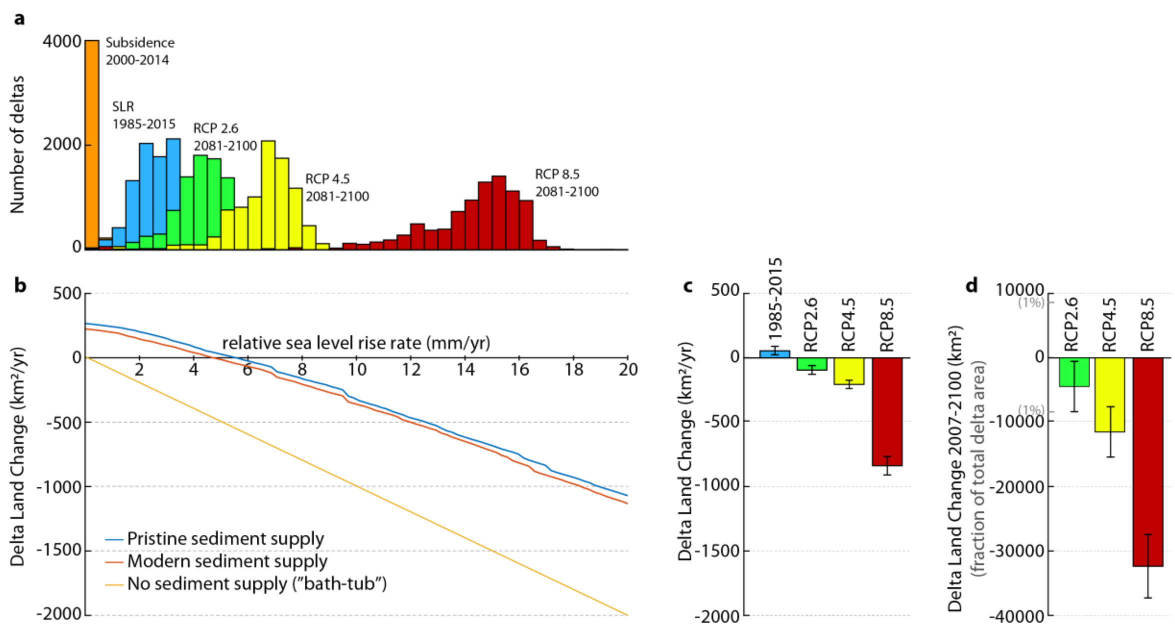

Figure 2: Effect of sea-level rise on delta land change. (**a**) Histogram of subsidence and sea-level rise rates for all coastal deltas, from (20, 21, 23). (**b**) Effect of sea-level rise rates on global delta land change for various fluvial sediment supply scenarios. (**c**) and (**d**) Land area change of all coastal deltas for past and projected RSLR, including subsidence for (**c**) 2081-2100 and (**d**) cumulative from 2007-2100.

Predictions of future delta change

Next, we predict the response of river deltas to future RSLR and sediment supply. Based on a global mean RSLR (Fig. 2b), present-day delta area gains will cease at a global scale if RSLR exceeds 5 mm yr^{-1}.

Delta area change is also affected by modifications to the fluvial sediment supply. From model assessments of the pristine (before river dams or land use change, see (24)) fluvial sediment supply to deltas, we find that the global reductions in sediment fluxes due to river damming have had a significant effect on delta land area change (Fig. 2b). Without anthropogenic modifications to the sediment supply feeding deltas, the threshold for net global delta land loss would have been 6 mm yr^{-1}.

In the limit of no fluvial sediment supply, our model predictions revert to a "bath-tub" response to RSLR -- passive flood mapping of coastlines without potential for sedimentation (Fig. 2b). Such bath-tub projections would estimate delta land loss of 370 km^2 $yr^{-1}$for 1985-2015, contrasting observed delta land gain of 54 km^2 yr^{-1}.

Future RSLR will vary regionally and depends on the RCP scenario. Following the recent SROCC predictions for sea-level rise under RCP8.5 (23) and assuming fluvial sediment supply and subsidence rates remain unchanged, we find that delta land loss will exceed 808 ± 80 km^2yr^{-1} (one s.d.) by the end of the century (2081-2100). Cumulative since 2007 to 2100, sea level rise under RCP8.5 will lead to the disappearance of about 32,000 ± 5,000 km^2 (one s.d.) of deltaic land – equal to about 4% of total delta area.

We also assess the relative importance of various drivers of delta change. First, model results suggest that without sea-level rise, river damming, deforestation, or subsidence, deltas would globally gain about 250 km^2yr^{-1}. This pristine delta growth rate compares well to a long-term perspective: modern total delta area (~900.000 km^2) divided by the age of modern delta initiation (~7500 yr) (25) corresponds to an average delta land area gain of about 120 km^2yr^{-1}.

Modern observed delta land gain of 54 km^2/yr (9) is substantially lower than under pristine conditions (Fig. 3a). We distinguish four drivers affecting delta growth: dams, deforestation, subsidence, and SLR, and compute expected delta area change if only one of these drivers were present. Model results suggests that, of those four drivers, dams and subsidence have dominated the observed reduction in delta land gain from 1985-2015 compared to pristine conditions (Fig. 3a).

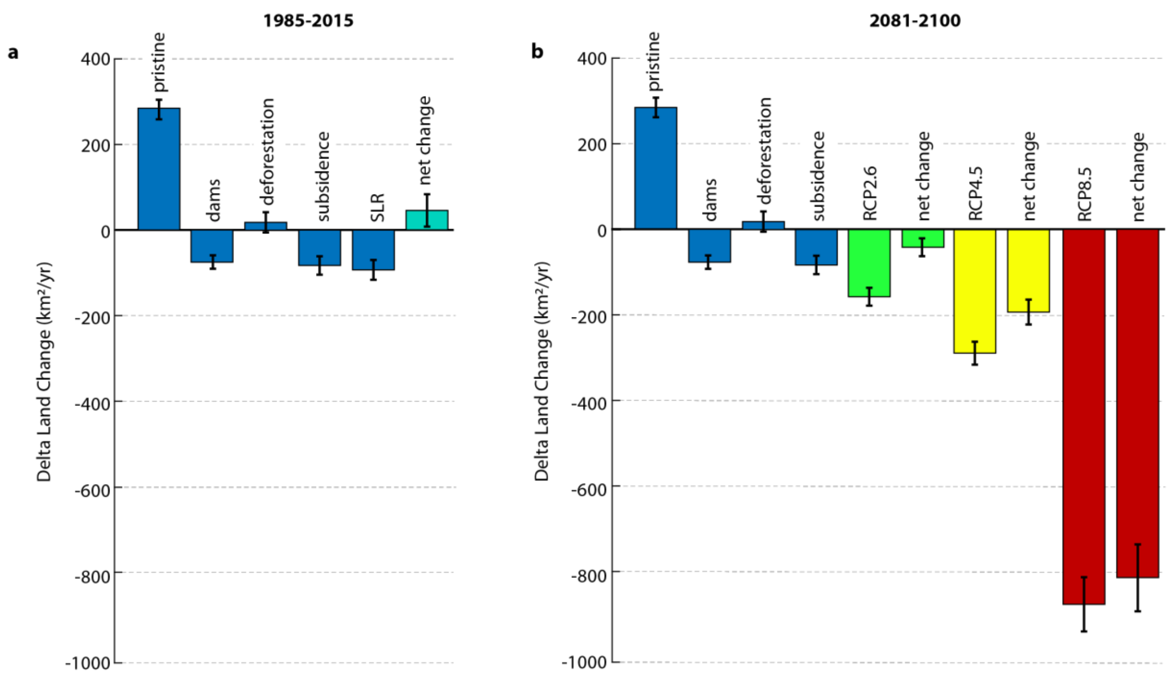

Figure 3: Relative influence of human drivers on delta change. Effect of different drivers of sediment supply or RSLR on delta growth, resulting in (**a**) net observed land gain from 1985-2015, and (**b**) projections of future delta change if the influence of dams, deforestation, and subsidence remain the same.

We also compare the influence of dams, deforestation, and subsidence on delta change to future rates of RSLR. By the end of the century, we find that the isolated effect of climate-change driver sea-level rise under RCP4.5 and RCP8.5 will greatly exceed other global drivers of delta land loss (Fig. 3b). Note that the non-linear effects that arise from the combination of different drivers tend to be small when considering all deltas globally (see Supplementary Materials).

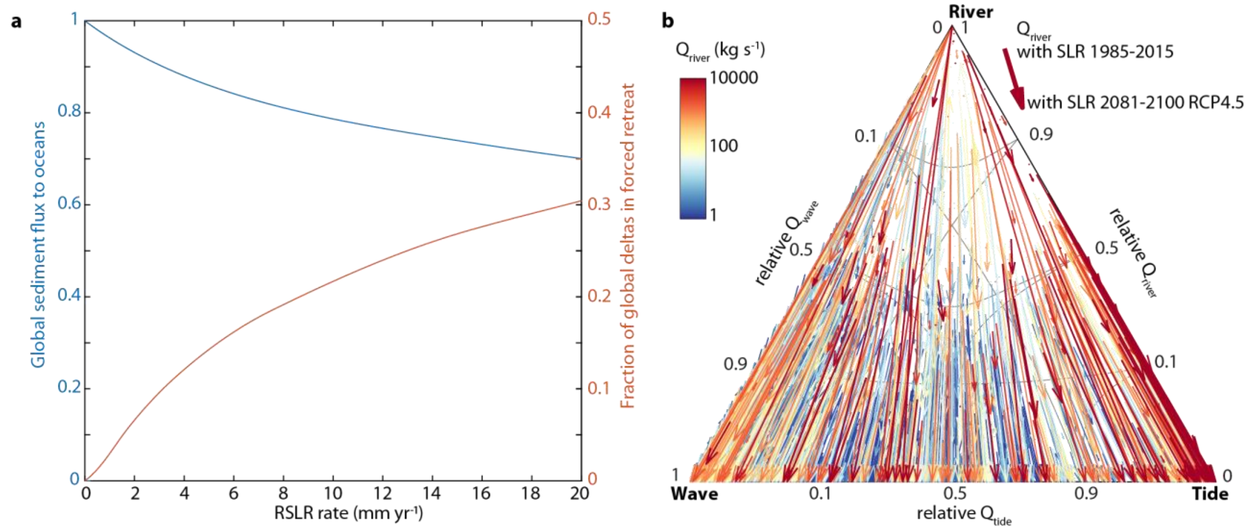

Figure 4: Effect of RSLR on delta morphology. (**a**) Effect of RSLR on (in blue) the global fluvial sediment flux to deltaic river mouths and (in red) the fraction of all coastal deltas where the river mouth is abandoned, and no fluvial sediment reaches the river mouth. (**b**) Effect of the reduced sediment flux to the river mouth on delta morphology, for SLR under RCP4.5 by 2100. Ternary diagram indicates relative influence of wave-, tidal- and fluvial sediment flux on delta morphology (9).

Besides a reduction of delta area, RSLR also affects delta plan-view morphology through its influence on the partitioning of fluvial sediment (2, 26). RSLR increases accommodation space and sediment deposition on the delta plain and lowers sediment delivery to the river mouth (2), which can make a delta more wave- or tide-dominated (9).

Our model suggests that for a global mean RSLR of 10 mm yr^{-1}, about 20% of the global fluvial sediment flux will be deposited on the delta plain (Fig. 4a). Such a RSLR rate would leave 80% of the fluvial sediment supply available at the river mouth for redistribution along coasts. Response to RSLR varies between deltas: following our model predictions for RCP8.5 by 2100, we predict that 18% of all coastal deltas will be in forced retreat (abandoned of all fluvial sediment supply at the river mouth). RSLR from 1985-2015 is expected to trap 9% of the global fluvial sediment supply onto the delta plain. This will increase to 22% by 2100 if emissions follow RCP8.5.

Using a new model for river delta morphology (9), we can investigate the effects of the projected reductions of the fluvial sediment flux for plan-view morphologic change (Fig. 4b). A decrease in fluvial sediment supply results in a shift in the delta sediment balance towards tidal and wave-driven sediment transport at the river mouth (9). Following our model simulations for RCP8.5 by 2100, we predict that 31% of all river dominated deltas will transform to wave- or tide-dominated deltas. Note that this is an equilibrium prediction towards which deltas will gradually adjust, and that our geomorphic model is not able to indicate a rate of delta change or detailed transient effects.

Although our simplified longitudinal profile model can capture broad global patterns of delta area change, accurate predictions for individual deltas remain challenging. Prediction accuracy is limited because of uncertainties in estimates of subsidence, sea-level change, fluvial sediment flux, and present-day morphology. Additionally, fluvial sediment supply and subsidence rates are unlikely to remain the same into the future. River damming is projected to overtake deforestation to further reduce fluvial sediment supply to deltas (27). Population pressure and associated groundwater withdrawal will likely increase subsidence rates in many densely populated deltas (28).

Other uncertainties stem from model assumptions. We assume a linear shoreline response to RSLR and sediment supply. Such a response may be justified for predictions on short timescales (~100 yrs) relative to the age of river deltas (~7500 yrs) (15). On the other hand, we also assume that delta morphodynamics can be expressed through a representative longitudinal profile –an assumption that typically only holds for long timescales or for small deltas. On short timescales, land area change from autogenic (free) delta morphodynamics such as avulsions or channel migration would likely obscure allogenic (forced) change (29) of an individual delta.

Our uncertainty assessment combines data and model errors and shows that our predictions are relatively robust when applied on a global scale. Additionally, our methods and data presented here provide quantitative and morphodynamic projections that offer an improvement over frequently used bath-tub models and agree with historic data on delta land area change.

Our predictions show substantial risk of land loss from climate-change driven RSLR. However, land loss is only one of the many hazards facing deltas (30). RSLR will also increase risks of coastal flooding, salinity intrusion, and river flooding. Although aggradation of the delta plain through fluvial sediment deposition can help to reduce climate-change driven risks, sedimentation is often prevented through the construction of flood protection levees. Recently, engineering approaches have been developed that prevent flood risk but also seek to mimic natural delta plain sedimentation (31, 32). Our results highlight that these approaches can protect deltas against some of the consequences of climate-change driven RSLR and should be encouraged.

References

1. R. M. Hoogendoorn, I. Overeem, J. E. A. Storms, Process-response modelling of fluvio-deltaic stratigraphy. *Comput. Geosci.* **34**, 1394–1416 (2008).
2. W. Kim, A. Dai, T. Muto, G. Parker, Delta progradation driven by an advancing sediment source: Coupled theory and experiment describing the evolution of elongated deltas. *Water Resour. Res.* **45**, W06428 (2009).
3. T. Muto, Shoreline Autoretreat Substantiated in Flume Experiments. *J. Sediment. Res.* **71**, 246–254 (2001).
4. W. Anderson, J. Lorenzo-Trueba, V. Voller, A geomorphic enthalpy method: Description and application to the evolution of fluvial-deltas under sea-level cycles. *Comput. Geosci.* **130**, 1–10 (2019).
5. M. D. Blum, T. E. Tornqvist, Fluvial responses to climate and sea-level change: a review and look forward. *Sedimentology* **47**, 2–48 (2000).
6. T. R. Anderson, *et al.*, Modeling multiple sea level rise stresses reveals up to twice the land at risk compared to strictly passive flooding methods. *Sci. Rep.* **8**, 14484 (2018).
7. J. Hinkel, *et al.*, Coastal flood damage and adaptation costs under 21st century sea-level rise. *Proc. Natl. Acad. Sci.* **111**, 3292–3297 (2014).
8. S. A. Kulp, B. H. Strauss, New elevation data triple estimates of global vulnerability to

sea-level rise and coastal flooding. *Nat. Commun.* **10**, 4844 (2019).

9. J. H. Nienhuis, *et al.*, Global-scale human impact on delta morphology has led to net land area gain. *Nature* **577**, 514–518 (2020).

10. J. Lorenzo-Trueba, V. R. Voller, C. Paola, A geometric model for the dynamics of a fluvially dominated deltaic system under base-level change. *Comput. Geosci.* **53**, 39–47 (2013).

11. J. B. Swenson, Fluviodeltaic response to sea level perturbations: Amplitude and timing of shoreline translation and coastal onlap. *J. Geophys. Res.* **110**, F03007 (2005).

12. W. Kim, C. Paola, V. R. Voller, J. B. Swenson, Experimental Measurement of the Relative Importance of Controls on Shoreline Migration. *J. Sediment. Res.* **76**, 270–283 (2006).

13. S. Y. J. Lai, H. Capart, Reservoir infill by hyperpycnal deltas over bedrock. *Geophys. Res. Lett.* **36**, L08402 (2009).

14. O. J. M. William Helland-Hansen, Shoreline Trajectories and Sequences: Description of Variable Depositional-Dip Scenarios. *SEPM J. Sediment. Res.* **66**, 670–688 (1996).

15. J. Lorenzo-Trueba, *et al.*, A similarity solution for a dual moving boundary problem associated with a coastal-plain depositional system. *J. Fluid Mech.* **628**, 427–443 (2009).

16. T. Muto, J. B. Swenson, Large-scale fluvial grade as a nonequilibrium state in linked depositional systems: Theory and experiment. *J. Geophys. Res.* **110**, F03002 (2005).

17. C. R. Hackney, *et al.*, River bank instability from unsustainable sand mining in the lower Mekong River. *Nat. Sustain.* **3**, 217–225 (2020).

18. M. Besset, E. J. Anthony, F. Bouchette, Multi-decadal variations in delta shorelines and their relationship to river sediment supply: An assessment and review. *Earth-Science Rev.* **193**, 199–219 (2019).

19. G. Donchyts, *et al.*, Earth's surface water change over the past 30 years. *Nat. Clim. Chang.* **6**, 810–813 (2016).

20. G. Erkens, E. H. Sutanudjaja, Towards a global land subsidence map. *Proc. Int. Assoc. Hydrol. Sci.* **372**, 83–87 (2015).

21. S. Dangendorf, *et al.*, Persistent acceleration in global sea-level rise since the 1960s. *Nat. Clim. Chang.* **9**, 705–710 (2019).

22. S. Cohen, A. J. Kettner, J. P. M. Syvitski, B. M. Fekete, WBMsed, a distributed global-scale riverine sediment flux model: Model description and validation. *Comput. Geosci.* **53**, 80–93 (2013).

23. M. Oppenheimer, *et al.*, "Sea Level Rise and Implications for Low-Lying Islands, Coasts and Communities" in *IPCC Special Report on the Ocean and Crysphere in a Changing Climate*, H. O. Portner, *et al.*, Eds. (IPCC, 2019).

24. S. Cohen, A. J. Kettner, J. P. M. Syvitski, Global suspended sediment and water discharge dynamics between 1960 and 2010: Continental trends and intra-basin sensitivity. *Glob. Planet. Change* **115**, 44–58 (2014).

25. D. J. Stanley, A. G. Warne, Worldwide Initiation of Holocene Marine Deltas by Deceleration of Sea-Level Rise. *Science* **265**, 228–231 (1994).

26. D. J. Jerolmack, Conceptual framework for assessing the response of delta channel networks to Holocene sea level rise. *Quat. Sci. Rev.* **28**, 1786–1800 (2009).

27. F. E. Dunn, *et al.*, Projections of declining fluvial sediment delivery to major deltas worldwide in response to climate change and anthropogenic stress. *Environ. Res. Lett.* **14**, 084034 (2019).

28. J. P. M. Syvitski, *et al.*, Sinking deltas due to human activities. *Nat. Geosci.* **2**, 681–686 (2009).

29. Q. Li, L. Yu, K. M. Straub, Storage thresholds for relative sea-level signals in the stratigraphic record. *Geology* **44**, 179–182 (2016).

30. Z. D. Tessler, *et al.*, Profiling risk and sustainability in coastal deltas of the world. *Science* **349**, 638–643 (2015).

31. J. H. Nienhuis, T. E. Törnqvist, C. R. Esposito, Crevasse Splays Versus Avulsions: A Recipe for Land Building With Levee Breaches. *Geophys. Res. Lett.* **45**, 4058–4067 (2018).

32. S. Temmerman, M. L. Kirwan, Building land with a rising sea. *Science* **349**, 588–589 (2015).

33. B. Lehner, K. Verdin, A. Jarvis, New Global Hydrography Derived From Spaceborne Elevation Data. *Eos, Trans. Am. Geophys. Union* **89**, 93 (2008).

34. USGS, Shuttle Radar Topography Mission. *Glob. L. Cover Facil. Univ. Maryland, Coll. Park. Maryl.* (2006).

35. C. Amante, B. W. Eakins, "ETOPO1 1 Arc-Minute Global Relief Model: Procedures, Data Sources and Analysis. NOAA Technical Memorandum NESDIS NGDC 24" (2009) https:/doi.org/10.7289/V5C8276M.

36. C. Paola, P. L. Heller, C. L. Angevine, The large-scale dynamics of grain-size variation in alluvial basins, 1: Theory. *Basin Res.* **4**, 73–90 (1992).

37. J. P. M. Syvitski, Y. Saito, Morphodynamics of deltas under the influence of humans. *Glob. Planet. Change* **57**, 261–282 (2007).

38. D. A. Edmonds, R. L. Caldwell, E. Brondizio, S. Siani, Coastal flooding will disproportionately impact people on river deltas. *pre-print* (2020) https:/doi.org/10.31223/osf.io/jdtp6.

39. N. Gorelick, *et al.*, Google Earth Engine: Planetary-scale geospatial analysis for everyone. *Remote Sens. Environ.* **202**, 18–27 (2017).

40. J. H. Nienhuis, A. J. F. T. Hoitink, T. E. Törnqvist, Future Change to Tide-Influenced Deltas. *Geophys. Res. Lett.* **45**, 3499–3507 (2018).

41. J. H. Nienhuis, A. D. Ashton, L. Giosan, What makes a delta wave-dominated? *Geology* **43**, 511–514 (2015).

42. J. X. Mitrovica, J. L. Davis, I. I. Shapiro, A spectral formalism for computing three-

dimensional deformations due to surface loads: 2. Present-day glacial isostatic adjustment. *J. Geophys. Res.* **99**, 7075 (1994).

43. J. A. Church, N. J. White, R. Coleman, K. Lambeck, J. X. Mitrovica, Estimates of the Regional Distribution of Sea Level Rise over the 1950–2000 Period. *J. Clim.* **17**, 2609–2625 (2004).

Acknowledgments

We thank Gilles Erkens for providing the global subsidence map and Sönke Dangendorf for the historical RSLR values. We thank Jorge Lorenzo-Trueba for helpful conversations about sea-level rise and deltas.

Funding

This research was supported by National Science Foundation award EAR-1810855, Netherlands NWO award VI.Veni.192.123, and American Chemical Society award PRF #59916-DNI8 to JHN and benefitted from the Water, Climate Future Deltas program of Utrecht University.

Author contributions

JHN conceptualized and performed the research. Both authors analyzed the results and wrote the paper.

Competing interests

Authors declare no competing interests

Data and materials availability

Model code and data to reproduce the findings and figures will be available post peer-review.

Materials and Methods

We estimate the effects of relative sea-level rise (RSLR) and fluvial sediment supply on all coastal deltas globally by applying a delta cross-sectional profile model. Our method involves (1) retrieving delta profiles, (2) analyzing the morphology of those profiles, (3) retrieving model boundary conditions (e.g. RSLR), (4) estimating effects of sea-level rise and sediment supply, (5) comparison against observed delta change, (6) translation of delta profile predictions to plan-view change, and (7) estimation of model and data uncertainty. All model data and code necessary to reproduce the results are available online.

1 Retrieval of delta profiles

We use the locations of 10,848 coastal deltas previously identified by Nienhuis et al (9). For each delta, we retrieve the subaerial channel profile from the HydroSheds accumulated drainage area data (ACC files) (33) that is based on SRTM data (34), both at a resolution of 15 arcsec. From the delta river mouth, we track elevation along the fluvial channel following a track of maximum drainage area up to 20 m above mean sea level (Fig. S1). For deltas above 60 degrees latitude, where HydroSheds is not available, we estimate subaerial delta profiles based on correlations of delta boundary conditions (river discharge and sediment supply (24)) with delta profiles of deltas below 60 degrees.

We use SRTM15+ for delta offshore profiles (35). SRTM15+ is a 15-arcsec global bathymetric map based on several global and regional digital data sets. For each river delta, we obtain an offshore profile by following a steepest descent path up to 500 m water depth. This results in 10,848 profiles covering between 10-100 km with a typical vertical accuracy of ~10 m (Fig. 1d).

2 Morphological analysis of delta profiles

We use the obtained channel and offshore profiles to estimate the effect of sea level rise and fluvial sediment supply on delta change (Fig. S1, Fig. S2). First, following (3, 15, 36), we fit a second-order polynomial across the entire subaerial (0-20 m) river profile, h_r (m),

$$h_r\ x\ = a_r x^2 + b_r x, \tag{1}$$

where we constrain a_r and b_r to be greater than zero.

We estimate the basement slope β from the slope at h_r (x_{15}) = 15 m,

$$\beta = 2a_r x_{15} + b_r. \tag{2}$$

Given the basement slope, the basement depth (h_b, m) under the river mouth is,

$$h_b = h_{15} - \beta x_{15}, \tag{3}$$

The horizontal distance of the river mouth to the basement (x_s, m) can then be obtained by,

$$x_s = \frac{h_b}{\beta}. \tag{4}$$

Next, following earlier work (3, 15), we fit a second-order polynomial to the delta profile up to 5 m,

$$h_d \;\; x \;\; = a_d x^2 + b_d x. \tag{5}$$

Based on our polynomial fits we can estimate the total longitudinal profile length of the river delta (x_s - x_r). This length controls the amount of potential sediment deposition on the subaerial delta and can be estimated by the minimum of (1) where the two polynomials (eq. 1 and 5) have the same slope, or (2) the location where they intersect,

$$x_r = x_s - \min\left(\frac{\beta - b_d}{2a_d}, \frac{b_r - b_d}{a_d - a_r}\right). \tag{6}$$

We also use the delta profile to estimate the slope at the river mouth (x = 0),

$$\alpha = b_d. \tag{7}$$

For the offshore profile, we fit a linear function through the first 100 meters to estimate the slope of the delta foreset,

$$h_s = \psi \cdot x. \tag{8}$$

We use the foreset slope to find the intersection of the basement and delta foreset. Based on the slope, we retrieve the horizontal distance to the delta toe,

$$x_t = \frac{h_b}{\psi - \beta}, \tag{9}$$

and the depth of the shoreface toe,

$$h_t = \frac{\psi \cdot h_b}{\psi - \beta}. \tag{10}$$

The delta longitudinal profile should be viewed as representative of a width-averaged delta. We estimate delta width based on an empirical regression of delta area from a compilation of 51 river deltas (R^2 =0.91, bias = 0) (37),

$$A_d = 10^6 \cdot 1.07 \cdot \frac{1}{D_{sh}} \cdot Q_w^{1.1} \cdot {Q_{s,sus}^{prist}}^{0.45}, \tag{11}$$

where A_d is delta subaerial surface area (m^2), D_{sh} is the depth of the continental shelf (m), $Q_{s,sus}^{prist}$ is the pre-dam suspended sediment flux (kg s^{-1}), and Q_w is the fluvial water discharge (m^3 s^{-1}). From A_d we approximate delta width (*w*, m) as the diameter of a circular delta area,

$$w = 2\sqrt{\frac{A_d}{\pi}}. \tag{12}$$

We acknowledge our approximation of delta width is crude. Therefore, we perform a sensitivity analysis of delta width and other relevant variables on our delta land area change predictions in section 8. We also include an estimated uncertainty of delta width into a Monte Carlo analysis of model and data uncertainty.

From our morphological analysis we obtain an estimate of length and width for each delta globally. Although these estimates are likely to be inaccurate for an individual delta, our combined estimate of global delta area of 885,000 km^2 compares well to an existing independent compilation of 847,000 km^2 from Edmonds et al (38).

3 Fluvial water and sediment discharge

For every delta we estimate the fluvial suspended and bedload sediment flux and water discharge. We obtain the fluvial suspended sediment load ($Q_{s,sus}$, kg s^{-1}) and water discharge (Q_w, m^3 s^{-1}) from WBMSed (22) (we refer to (9) for details). WBMSed is an empirical model that uses observed relations between measured fluvial sediment transport and climate, soil type, elevation, and other parameters to make global gridded predictions of the fluvial sediment flux for all rivers. Using calibration techniques based on sediment flux data in human influenced and pristine river systems, WBMSed generates estimates of pristine (natural, $Q_{s,sus}^{prist}$) and disturbed (modern, including effects of e.g. land use changes and river damming, $Q_{s,sus}^{dist}$) fluvial sediment supply. Fluvial sediment and water discharge data can be considered representative of the conditions at the delta apex, upstream of delta distributary networks.

We obtain a width-averaged fluvial sediment flux based on our delta width estimate, which we report in units of m^2/yr,

$$q_{s,sus} = \frac{Q_{s,sus}}{w}, \tag{13}$$

such that $q_{s,sus}^{prist}$ and $q_{s,sus}^{dist}$ are the disturbed and pristine width-averaged fluvial sediment flux, respectively.

We are not aware of global estimates of the bedload sediment flux to each delta. Therefore, we estimate the bedload flux based on the shape of the modern delta profile. Earlier studies (15, 36) have shown that fluvial bedload $q_{s,bed}$ (m^2/yr) can be estimated by,

$$q_{s,bed} = \beta \cdot R_{ab} \cdot \nu, \tag{14}$$

where β is the basement slope, $\nu = \frac{1}{2} Q_w / w$ is the diffusivity of the fluvial longitudinal profile (m^2/yr) (36), and R_{ab} is the ratio of the alluvial and basement longitudinal slopes at the upland-delta transition (Fig. S2). There are two ways of retrieving R_{ab} directly from the delta profile (15). The first method uses the delta cross-sectional volume ratio upstream and downstream of the delta-basement origin,

$$R_{ab} = \ 2 \quad x_s - x_r \quad \cdot a_d + b_d \ \ /\beta. \tag{15}$$

R_{ab} can also be estimated based on the relative volumes of the subaerial and subaqueous delta (15),

$$R_{ab} = \frac{\phi}{\phi + \ 1 - \phi \ \frac{x_t}{x_t - x_r}}, \tag{16}$$

where $\phi = \frac{-x_r}{x_s - x_r}$. In our analysis we estimate R_{ab} by taking the average of the two (eq. 15 and eq. 16) estimates.

For all deltas globally we find a bedload sediment supply of $0.89 \cdot 10^9$ m^3 yr^{-1} and a (modern) suspended load supply of $8.6 \cdot 10^9$ m^3 yr^{-1}. Combined, we estimate the fluvial sediment flux (m^2/yr) as,

$$q_{s,tot} = q_{s,bed} + f_r \cdot q_{s,sus}, \tag{17}$$

where f_r is the fraction of sediment retained in the delta profile. For the purpose of this study we assume $f_r = 1$. We do not vary the bedload sediment flux estimates between pristine and disturbed conditions.

4 Relative sea level rise

For every delta we retrieve local subsidence z_{sub} (m/yr) and sea-level rise z_{slr} (m/yr) rates (Fig. S3), which together add up to relative sea-level rise (RSLR),

$$z_{rslr} = z_{sub} + z_{slr}. \tag{18}$$

For past (1985-2015) z_{slr}, we use a combination of tide-gauge and satellite altimetry data from (21). These data are available on a 1-degree grid. We find the closest data point to each river delta and fit a linear trend through these data to obtain a time-averaged z_{slr}.

We estimate subsidence rates from a global subsidence model (20). These data are available on a 5 arc-min grid. We apply a 5-cell smoothing algorithm and then extract the data closest to each river delta. Subsidence in this model is estimated for the period 2000-2014, but here we assume this period characterizes average subsidence rates for the 1985-2015 period. Details on model and data uncertainty can be found in Supplementary Materials section 6.

For future z_{slr} we obtain estimates for different RCP scenarios from the recent SROCC report (23). We find the nearest data for each delta from the 1-degree grid and extract z_{slr} for RCP 2.6, 4.5, and 8.5 for end-of-century rates (2081-2100) as well as total (2007-2100) future z_{slr}. For assessment of future RSLR we use the 2000-2014 subsidence rates. Note that these will likely be conservative as increased groundwater withdrawal will likely speed up subsidence in many deltas (28).

4 *Morphologic model of delta change*

We estimate delta land area change by comparing sediment supply feeding the delta with the creation of accommodation space on the delta topset (from RSLR). RSLR will move x_r upstream at a rate (m/yr) of,

$$x_r = -\frac{z_{rslr}}{\beta}, \tag{19}$$

and move the shoreline x_s at a rate (m/yr) of,

$$x_s = \begin{cases} \max\left(\frac{q_{s,tot} - v_{rslr}}{z_{rslr}}, \frac{z_{rslr}}{\alpha}\right), & \text{if } z_{rslr} > 0 \text{ and } q_{s,tot} < v_{rslr} \\ \frac{q_{s,tot} - v_{rslr}}{h_t}, & \text{if } z_{rslr} > 0 \text{ and } q_{s,tot} > v_{rslr}, \\ \frac{z_{rslr}}{\alpha} + \frac{q_{s,tot}}{h_t}, & \text{if } z_{rslr} < 0 \end{cases} \tag{20}$$

where $v_{slr} = \ x_s - x_r \ \cdot z_{rlsr}$ (m^2/yr) is the creation of accommodation space on the delta top by the rising sea, $z_{rslr} = \int z_{rslr}\ dt$ (m) is the change in relative sea-level over the considered time interval. Multiplied by delta width, the predicted delta area change (m^2/yr) is then equal to,

$$A_{pred} = w \cdot x_s, \tag{21}$$

which can be easily assessed for different RSLR, fluvial sediment supply, effective sediment retention fractions, or delta morphologies (Fig. S5). Note that we ignore delta land gain along the upstream boundary in our assessment of delta land area change, because it constitutes land conversion from existing (albeit non-deltaic) land. We also do not run a time-dependent model but instead estimate land gain or land loss as an instantaneous change from the modern delta profile. This is unlikely to constitute a major source of error because the timeframe of our predictions is short (~100 yrs) compared to the age of river deltas (~7500 yrs).

5 *Comparison against observed delta change*

For the years 1985-2015, we compare A_{pred} to observations of delta land area change, A_{obs}. We use data from (9), who employ the Google Earth Engine (39) to extract delta surface area change based on Landsat data and the Deltares Aquamonitor (Fig. S1, Fig. S3a) (19). The total net deltaic land area gain for the 10,848 deltas within the dataset is 54 ± 12 (2 s.d.) km^2/yr.

Comparing observed vs. predicted delta area change for 10,848 deltas we obtain a goodness-of-fit (r^2) of 0.4. We find a Skill Score of 0.2, defined as,

$$SS = 1 - \frac{\sum_{i=1}^{n}\left(A_{obs,i} - A_{pred,i}\right)^2}{\sum_{i=1}^{n}\left(A_{obs,i} - \overline{A_{obs,i}}\right)^2}. \tag{22}$$

where n is the number of river deltas (10,848) (Fig. S4a).

The correlation coefficient is low for several reasons: (1) the model is uncalibrated, (2) our model complexity is low and includes only a limited number of variables, (3) there is likely to be significant error in the model forcing (e.g. RSLR, fluvial sediment supply) as well as in our estimate of observed land area change, and (4) there are many (small) deltas for which the 30-year (1985-2015) period is short relative to other delta dynamics. When we compare our predictions against observations for only large deltas (e.g. 1% of deltas with the largest fluvial sediment supply) we find an improved goodness-of-fit (Fig. S4b) We refer to Supplementary Materials section 7 where we describe our Monte Carlo analysis to quantify the effect of these uncertainties on our model results.

6 *Translation to geomorphic change*

We investigate the effect of RSLR on the fluvial sediment supply to deltaic river mouths. For high RSLR, a substantial fraction of the fluvial sediment supply will be trapped on the delta top. The sediment supply rate that remains and it delivered to the river mouth can be estimated by,

$$q_{s,rm} = \max(0, q_{s,tot} - \ v_{slr}), \tag{23}$$

where $v_{slr} = \ x_s - x_r \ \cdot z_{rlsr}$ (m^2/yr) is the creation of accommodation space on the delta top by the rising sea. Note that we neglect the small increase in the delta topset that will be created through delta progradation independently of RSLR.

Next, we assess the relative magnitude of the fluvial sediment supply at the river mouth ($Q_{s,rm} = \ q_{s,rm} \cdot w$) vs. tide- and wave-driven transport at the river mouth. Tide-driven sediment transport refers to the transport of sediment in and out of the river mouth by tide-driven water discharge (40). Wave-driven transport refers to the maximum potential alongshore transport of fluvial sediment away from the river mouth (41). Changes to the relative balance of river, wave, or tide-driven transport at the river mouth will result in delta morphologic change. A decrease in fluvial transport towards the river mouth (e.g., because of upstream trapping by RSLR) can therefore lead to a decrease in delta protrusion if waves increase their dominance. It can lead to siltation and narrowing of deltaic channels when tides increase their dominance. We refer to Nienhuis et al. (9), for details and data of these sediment fluxes.

7 Uncertainty analysis

We assess model and data uncertainty through a Monte Carlo analysis. We use random sampling of the model input variables to predict delta area change (Table S1). We repeat this process 5000 times to generate a probability distribution of delta area change, which gives an indication of the sensitivity of our predictions to model and data uncertainty. The reported uncertainties in our results represent the standard deviation of the Monte Carlo probability distribution.

We also assess the sensitivity of delta area change predictions to variations in individual model parameters (Fig. S6). We find that the results are sensitive to estimates of delta width, delta toe depth, delta plain diffusivity, and delta length. These sensitivities highlight that our model predictions are highly uncertain for individual deltas and should primarily be used for large-scale (global) delta change assessment.

Supplementary Figures and Tables

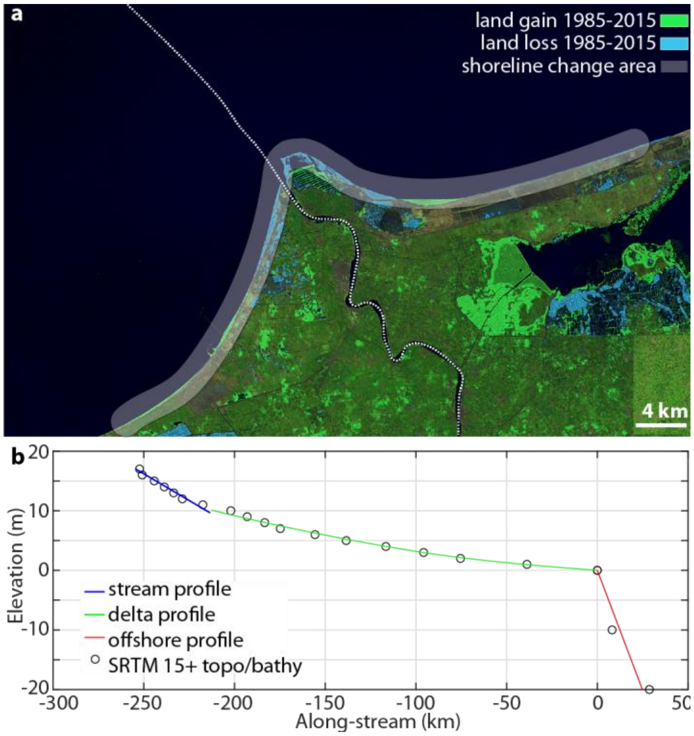

Figure S1. Example of data retrieval for the Nile Delta, Egypt. (**a**) Landsat image including the delta fluvial and offshore profile, overlaid by AquaMonitor (19) data of recent surface water change (see Supplementary Materials section 5). (**b**) Elevation along the fluvial and offshore profile, including estimated upstream, delta, and offshore slopes (see Supplementary Materials section 2).

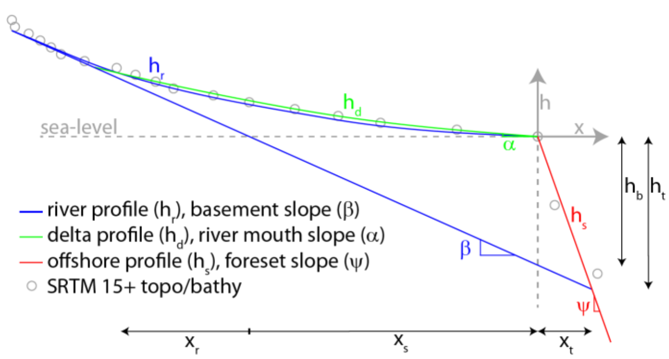

Figure S2. Schematic delta longitudinal profile.

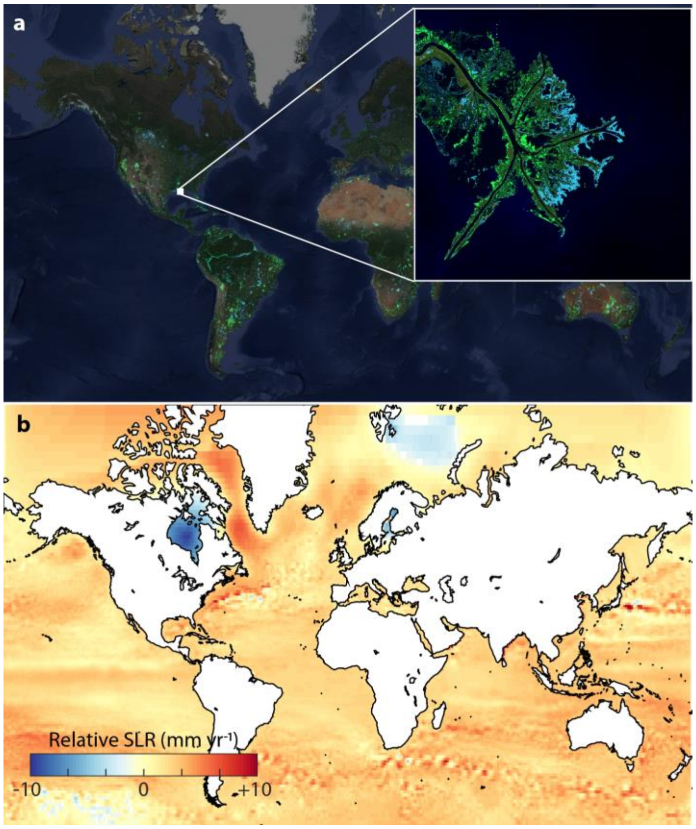

Figure S3. (**a**) AquaMonitor (19) data of recent surface water change, inset shows the mouth of the Mississippi River Delta. (**b**) RSLR change from 1985-2015, combining subsidence (20) and sea-level change data (21), and assuming RSLR of -10 mm/yr for Hudson Bay (42).

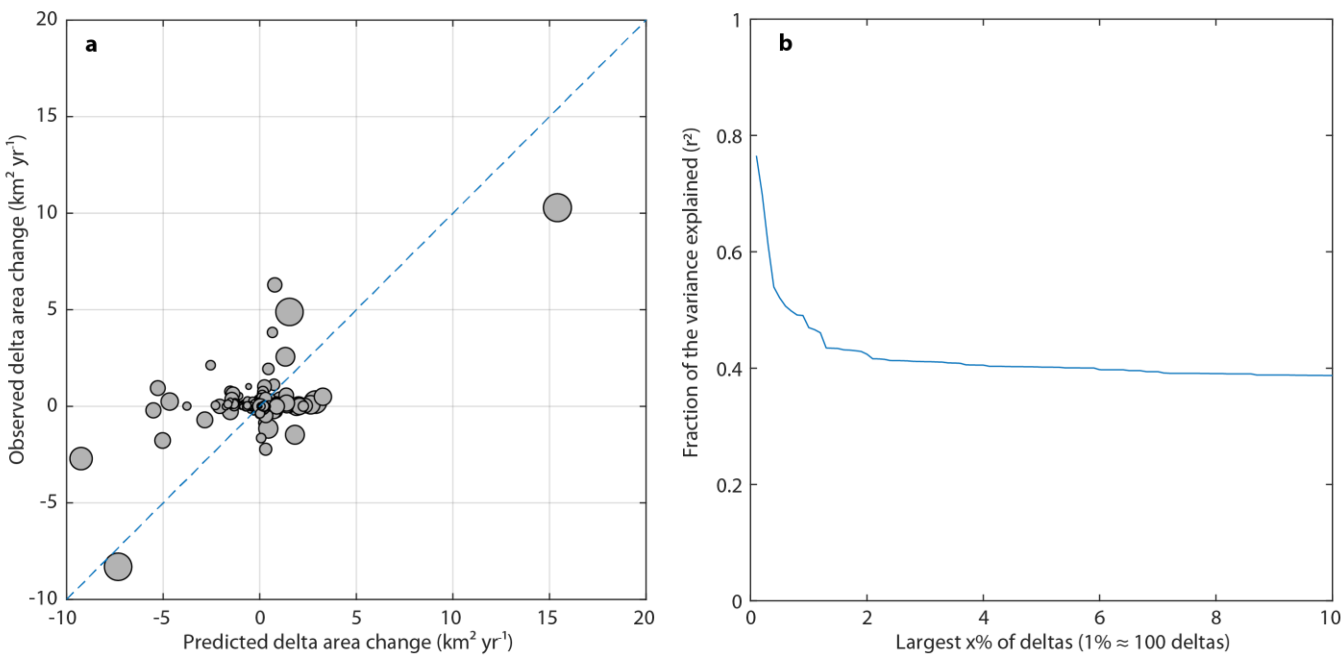

Figure S4. (**a**) Comparison of predicted and observed annual delta area change for 1985-2015. Markers represent individual deltas and marker size scales with the fluvial sediment supply, a proxy for delta size. (**b**) Regression coefficient for subsets of all deltas, showing increased predictive capability for larger deltas.

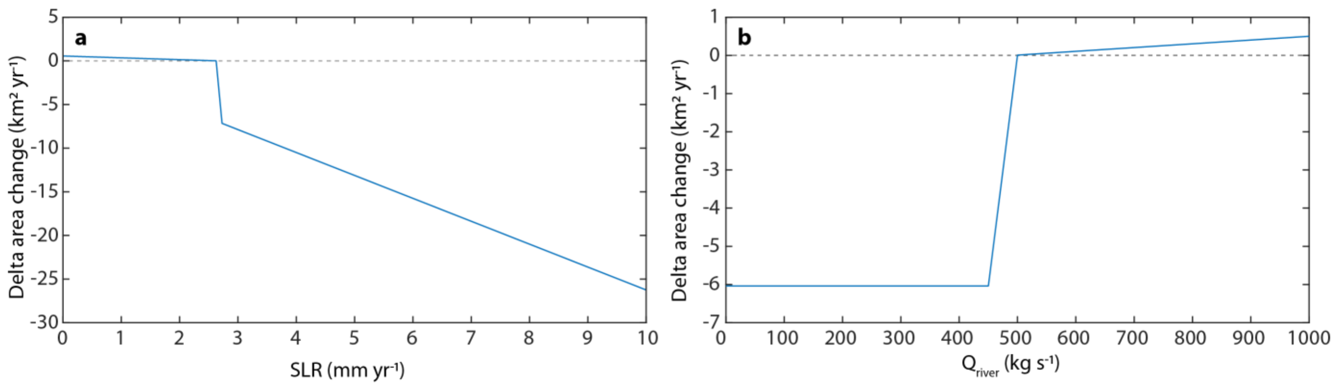

Figure S5. Example model prediction for an individual delta, (**a**) for varying RSLR and (**b**) varying fluvial sediment supply. Deltas are sensitive to RSLR and fluvial sediment supply in their transition from progradation (land gain) to erosion (land loss).

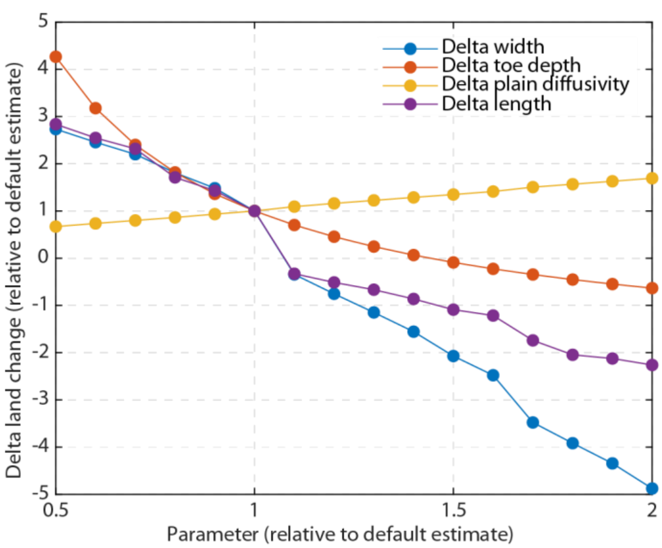

Figure S6. Sensitivity of delta area change estimate to delta morphological parameters, rescaled to indicate value compared to their default estimate.

Table S1. Model and data variables and their assumed distribution used as input for the Monte Carlo analysis.

Variable	**Assumed distribution**	**Assumed range**	**Source**
Sea level rise 1985-2015	normal	Standard deviation of 0.3 mm/yr	(43)
Sea level rise 2007-2100	normal	Regionally varying standard deviation equal to high uncertainty estimate from data	(23)
Subsidence 2000-2014	uniform	Subsidence model prediction ± 50%	
Delta width (w)	uniform	Delta width prediction ± 50%	
Delta toe depth (h_t)	uniform	Delta toe depth estimate ± 50%	
Fluvial suspended load supply ($q_{s,sus}$)	uniform	Fluvial supply model prediction ± 38%	(22)
Fluvial bed load supply ($q_{s,bed}$)	uniform	Fluvial bed load prediction ± 50%	
Fluvial profile diffusivity (v)	uniform	Fluvial diffusivity prediction ± 50%	